Axial Development of Diesel Sprays at Varying Ambient Density

Alan L. Kastengren, Christopher F. Powell
Center for Transportation Research
Argonne National Laboratory
Argonne, IL 60439 USA

Zunping Liu, Seoksu Moon, Jian Gao, Xusheng Zhang, and Jin Wang
Advanced Photon Source
Argonne National Laboratory
Argonne, IL 60439 USA

Abstract

Due to their importance in the performance and emissions of diesel engines, diesel sprays are the subject of significant research interest. One of the most fundamental findings of this research has been that the width of sprays is strongly dependent on the density of the ambient gas environment. There is disagreement in the literature, however, concerning the quantitative relationship between spray width and ambient density. A limitation in these previous studies is the use of optical diagnostics, which focus on the periphery of the spray.

X-ray radiography is a well-established technique to probe the internal structure of transient diesel sprays. Unlike optical techniques, it can provide quantitative data regarding the mass distribution of dense sprays. Previous x-ray radiography work examining the relationship between ambient density and spray width showed that, similar to variable-density gas jets, a rescaling of the spray axial coordinate to account for the density ratio between the jet and ambient fluids can account for much of the variation in spray width with ambient density. A limitation of this previous work was the limited field of view available for the x-ray radiography measurements, particularly for the low ambient density cases. The current work examines the influence of ambient density on diesel spray structure over an expanded range. A smaller nozzle and larger windows have been used compared to previous x-ray radiography work, allowing more firm conclusions to be drawn regarding the applicability of axial rescaling to account for ambient density effects. The spray mass distribution, width, and mass-averaged velocity will be examined to understand the influence of ambient density and to better understand how quickly the spray approaches the behavior of a self-similar jet.

Nomenclature

M = Projected density, µg/mm^2
R = Ratio of fuel density to ambient gas density
d_0 = Nozzle diameter, µm
x = Axial distance from the nozzle, mm
x' = Axial distance from nozzle divided by $R^{1/2}$, mm
x* = Rescaled axial distance from nozzle, $x/(d_0R^{1/2})$
y = Transverse distance from spray nozzle axis perpendicular to beam direction, mm
z = Transverse distance from spray nozzle axis along beam direction, mm
ρ_f = Density of liquid fuel, kg/m^3
ρ_a = Ambient gas density, kg/m^3

Introduction

Due to their importance in the performance and emissions of diesel engines, diesel sprays are the subject of significant research interest. The high optical density of diesel sprays has limited investigations of near-nozzle spray structure. Numerous studies have examined the spatial extent (axial and transverse) of sprays under varying conditions [1-3]. Other measurements have examined the entrainment of ambient gases into the spray [4,5]. As the spray becomes more dilute at more downstream positions, additional diagnostics can be used. However, few diagnostics can probe diesel sprays in the near-nozzle region [6-8], and even fewer can provide quantitative data regarding spray structure.

X-ray radiography is a well-established technique to probe the internal structure of transient diesel sprays. X-rays tend to be absorbed by sprays, rather than scattered. Thus, unlike optical techniques, x-ray techniques can provide quantitative data regarding the mass distribution of dense sprays. The use of the high-intensity, monochromatic x-rays available at synchrotron x-ray sources has allowed time-resolved measurements of gasoline and diesel spray structure to be performed [9,10].

One of the most fundamental findings of previous diesel spray research has been that the width of sprays is strongly dependent on the density of the ambient gas environment. This relationship is generally given as a power-law relationship between the spray cone angle (or tangent of the cone angle) and the density ratio between the liquid and ambient gas. There is disagreement in the literature, however, concerning the exponent of this power law [3,11-13].

Previous x-ray radiography work [14] examining the relationship between ambient density and spray width in diesel sprays showed that, similar to variable-density gas jets [15], rescaling the spray axial coordinate by the square root of the density ratio between the jet and ambient fluids can account for much of the variation in spray width with ambient density. A limitation of this previous work was the limited field of view available for the x-ray radiography measurements, particularly for the low ambient density cases. Due to the nature of the rescaling, a given axial distance in physical space represents less of the axial spray development at lower ambient density. To truly compare spray behavior at various density values, data is needed over a longer axial extent at low ambient density than at high ambient density.

The current work extends the previous work on the influence of ambient density on diesel spray structure. An expanded range of axial positions is examined, particularly for low ambient density. The shape of the mass distributions at different axial distances from the nozzle will be compared for different ambient densities to demonstrate how the jet approaches self-similar behavior. Three-dimensional reconstructions of the spray density will be used to test the limits of the applicability of the axial rescaling to explaining spray structure. Finally, trends in the axial velocity for different injection and ambient density conditions will be examined.

Experimental Method

The experiments in this work were performed at the 7-BM x-ray beamline at the Advanced Photon Source. A detailed description of the beamline is given elsewhere [16]. The beamline produced a spatially broad beam of high-intensity x-rays at 8 keV photon energy with a relatively narrow spectral bandwidth (1.4% $\Delta E/E$). The x-ray beam was focused using a pair of 100 mm long focusing mirrors in a Kirkpatrick-Baez geometry [17]. The nominal mirror angle for these measurements was 7 mrad, and the focus distance from the center of the vertical focusing mirror was 140 mm. A pair of slits before the focusing mirrors limited the x-ray beam size entering the mirrors to 0.5 mm x 0.5 mm. The measured focal spot size was 9 µm vertically x 9 µm horizontally full width at half maximum (FWHM). The focused x-ray beam passed through a pressurized spray chamber with x-ray transparent windows. The transmitted x-ray intensity was monitored with an avalanche photodiode (APD). The signal from the APD was recorded at 1 GHz by a Yokogawa DL7200 oscilloscope.

The sprays examined in this work were produced by a Bosch CRIP 2.2 injector fitted with a custom-made axial single-hole nozzle with a nominal diameter of 110 µm. The nozzle has been hydroground to a discharge coefficient of 0.86. The fuel used is a diesel calibration oil (Viscor 1487) with a cerium-containing additive to improve the x-ray contrast. The fuel density is 884 ± 3 kg/m^3, and the fuel mass absorption coefficient was 2.504 x 10^{-3} m^2/g. The spray repetition rate was approximately 3 Hz.

The fuel was injected into a spray chamber filled with nitrogen gas at room temperature and elevated pressure. Experiments were performed at 5 bar and 20 bar absolute chamber pressure, corresponding to 5.6 kg/m^3 and 22.5 kg/m^3 ambient density, respectively. Due to the limited size of the x-ray transparent windows, the measurements at 20 bar chamber pressure ranged from 0.1 mm to 16 mm downstream of the nozzle. Larger windows were used for the measurements at 5 bar chamber pressure, allowing measurements from 5 to 30 mm downstream of the nozzle. For all experiments, a purge flow of nitrogen gas (2-2.5 L/min) was maintained to clear the spray chamber of stray fuel droplets.

The x-ray transmission through the spray was measured at one position at a time. At each measurement point, 32-128 individual spray events were averaged to increase the signal/noise ratio of the measurements. The temporal resolution of the processed data was 3.68 µs, which corresponds to the cycle time of the x-ray source. After processing, the standard deviation of the individual projected density measurements was approximately 1.3 µg/mm^2. A large number (1400-2000) of measurement points were combined to measure the full two-dimensional spray fuel mass distribution as a function of time. Examples of the measurement grids for the measurements at 5 bar and 20 bar chamber pressure are given in Figs. 1 and 2.

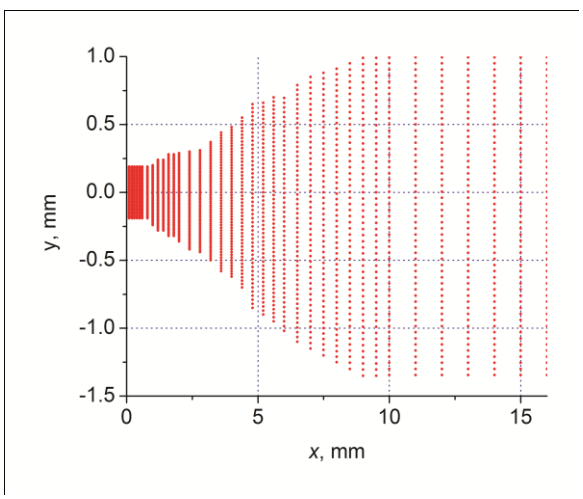

Figure 1. Example measurement grid at 22.5 kg/m^3 ambient density.

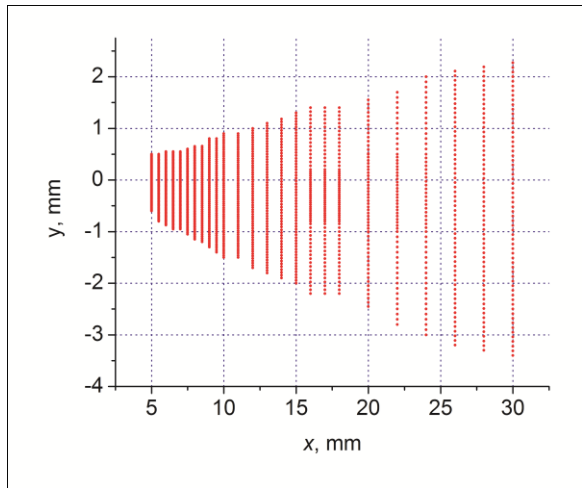

Figure 2. Example measurement grid at 5.6 kg/m^3 ambient density.

Results

While the x-ray radiography data for these sprays shows a great deal of transient structure, this work will focus exclusively on the "steady state" structure of the spray. For the measurements shown in this work, to further reduce the level of noise in the data, the data were binned for 25 time steps, corresponding to averaging across 92 µs (equivalent to 1.1° CA at 2000 rpm).

Spray Self-Similarity

In single-phase jets, the jet behavior becomes self-similar at large distances from the nozzle. When the jet becomes self-similar, transverse profiles of velocity or concentration maintain the same shape at different downstream distances; only the scaling of the distribution changes. As a diesel spray becomes more dilute and more closely resembles a single-phase jet, it is logical that its behavior will converge toward self-similar behavior far from the nozzle.

To examine the approach of the sprays to self-similarity using radiography data, an expression for the scaling of the projected density must be developed. For single-phase turbulent jets [18], the local jet velocity and passive scalar concentration scale as $1/x$ and the transverse coordinate scales as x. Let the spray density ρ be given by:

$$\rho(x,y,z) = \frac{C(\xi,\eta)}{x}$$
$$\xi = \frac{y}{x} \qquad (1)$$
$$\eta = \frac{z}{x}$$

where $C(\xi,\eta)$ gives the nondimensional density profile in the self-similar region. The projected spray density is an integral in the beam (z) direction.

$$M(x,y) = \int \frac{C(\xi,\eta)}{x} dz$$
$$= \int \frac{C(\xi,\eta)}{x} x d\eta \qquad (2)$$
$$= \int C(\xi,\eta)\, d\eta$$

The integral is a function only of the self-similar density profile. Thus, if the jet is fully developed, the projected density should be constant at constant ξ even as x is varied. For example, the peak projected density should remain constant; only the width of the distribution will change.

To investigate the approach of the spray behavior to self-similarity, Fig 3 shows the transverse distributions of projected density at several nondimensional distances x^* from the nozzle at 22.5 kg/m^3 ambient density. The transverse coordinate has been scaled with x', the axial coordinate normalized with the square root of the density ratio R. Several trends are evident. First, the rescaling of the transverse coordinate is relatively effective at scaling the spray width. This is reflected in the Figure by the fact that the rescaled data have similar widths, and indicates that the spray spreads somewhat linearly. However, the shape of the transverse distribution undergoes substantial development as x^* increases. At positions near the nozzle, the transverse distribution shows a severely skewed appearance, with a secondary peak on the negative y side of the distribution. This appearance is likely due to imperfections in the nominally axisymmetric nozzle geometry. At more downstream positions, the peak projected density decreases, and the distribution becomes smoother, indicating that the turbulent mixing in the spray is making the fuel concentration distribution more uniform. The density on the edges of the distribution also increases as the jet develops.

A similar figure is shown for 5.6 kg/m^3 ambient density in Fig. 4, with the transverse projected density distributions given at the same x^* values as in Fig. 3. There are several similarities between the two plots. The density distribution is clearly asymmetric at the most upstream positions, with the character of the asymmetries matching that seen at higher ambient density. The projected density also decreases as the fluid moves downstream, indicating that the jet is still developing throughout the region shown in this figure. The distributions also become smoother at more downstream positions, with a more gradual transition from the high-density peak to the low-density edges of the distribution. Similar to the high pressure case, the rescaling of the transverse coordinate is effective at scaling the spray width, an indication that the spray spreads somewhat linearly.

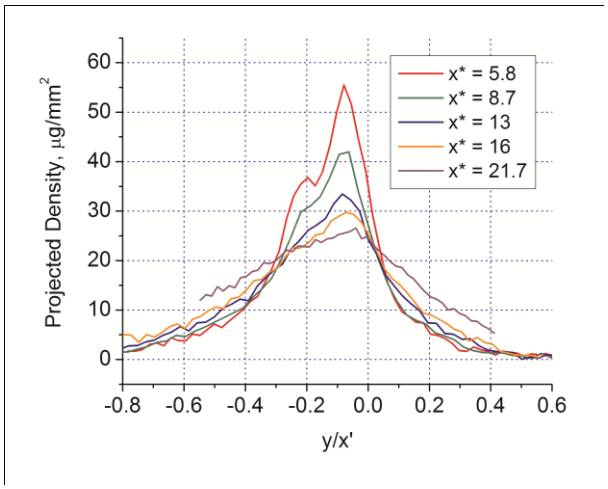

Figure 3. Transverse distributions at various x* for 1100 bar rail pressure, 700 µs injection duration, and 22.5 kg/m^3 ambient density.

There are, however, some marked differences between the two ambient density conditions plotted in Figs. 2 and 3. The distributions are wider at lower ambient density; note the different horizontal scales for the two figures. (For clarity, this refers to the width *after* accounting for the ambient density; at a given x, the distributions are narrower at lower ambient density.) The projected density values are also significantly lower at lower ambient density. Finally, the asymmetries in the projected density distributions remain evident much farther downstream for the low ambient density case than for the high ambient density case.

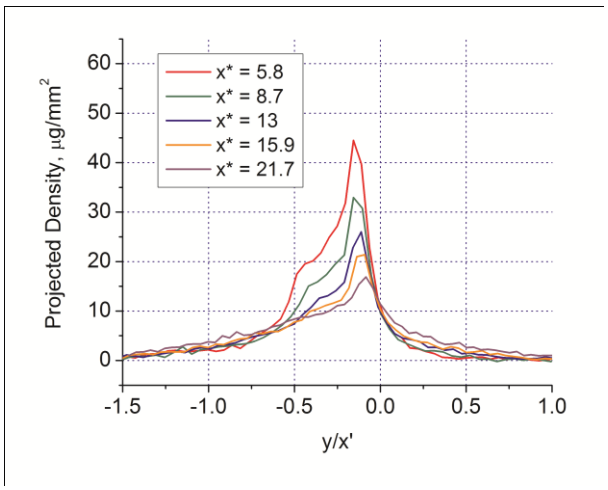

Figure 4. Transverse distributions at various x* for 1100 bar rail pressure, 700 µs injection duration, and 5.6 kg/m^3 ambient density.

Trends in Spray Width

Previous work [14] has shown that rescaling the axial distance from the nozzle with the square root of

the density ratio explains much of the variation in spray width with ambient density. The limited field of view of these measurements at low ambient density made it difficult to confirm the validity of this rescaling far from the nozzle. A plot of the FWHM of the spray vs. x from the current study is shown in Fig. 5. Clearly, higher ambient density causes the spray to spread much more rapidly than at low ambient density, as expected from previous work.

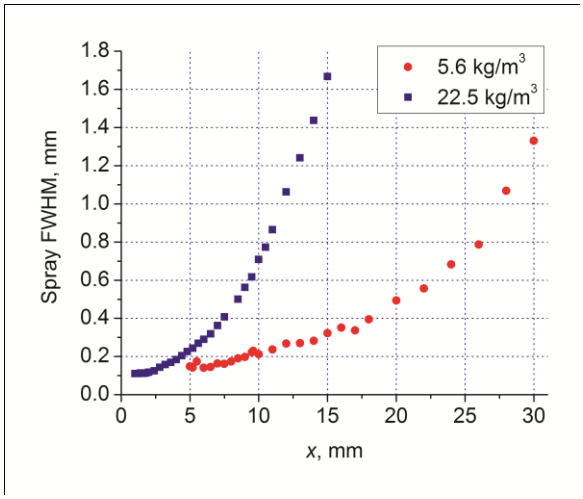

Figure 5. FWHM of the spray mass distribution vs. x at steady state for 5.6 kg/m^3 and 22.5 kg/m^3 ambient density.

If the axial coordinate is rescaled, the trends become more similar. Figure 6 shows the spray FWHM vs. x^*. The spray widths match quite well for $x^* < 10$. For $x^* > 10$, the spray FWHM is narrower for low ambient density than at high ambient density, even when rescaled. This may be partially caused by the different qualitative shape of the transverse distributions at the two ambient densities, as shown in Figs. 3 and 4. Perhaps a more robust definition of spray width is needed to make more detailed comparisons. Nevertheless, the axial rescaling still accounts for much of the variation in spray width with ambient density.

Further insight regarding the spray behavior can be made by plotting the FWHM normalized by the nozzle diameter and x^* (i.e., FWHM / d_0 / x^*). If the spray is fully developed and spreading linearly, this value should be independent of x^*, aside from a correction for the virtual origin of the spray, which is not accounted for here. As shown in Fig. 7, however, this quantity is by no means constant with respect to x^*. This serves to further illustrate that the spray mass distributions are undergoing significant development throughout the measurement range of this study.

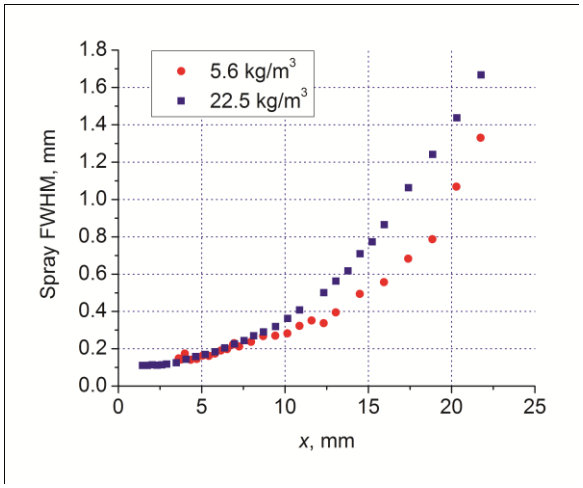

Figure 6. FWHM of the spray mass distribution vs. x^* at steady state for 5.6 kg/m^3 and 22.5 kg/m^3 ambient density.

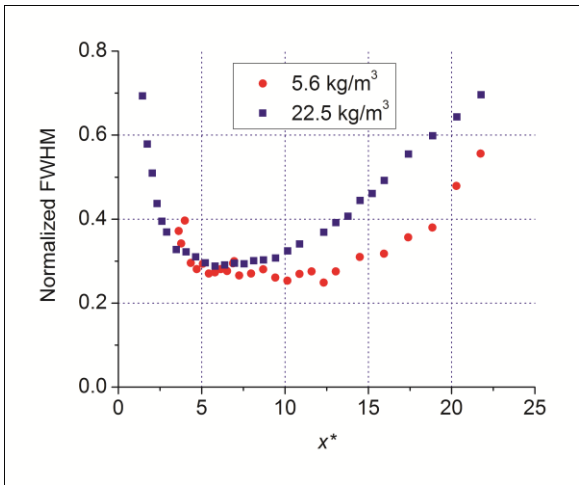

Figure 7. Rescaled FWHM vs. x^* at steady state for 5.6 kg/m^3 and 22.5 kg/m^3 ambient density.

Three-Dimensional Spray Density Reconstruction

Radiography by its nature is a pathlength-integrated measure of spray density. The radiography measurements give a two-dimensional projection of the three-dimensional spray density distribution. Tomography can be used to mathematically reconstruct the three-dimensional spray distribution. Tomography, however, depends on measuring the spray from many (tens to hundreds) of viewing angles [19]. The time required for each two-dimensional projection (approximately 24 hours for a single view) and the limitations of the current spray chamber geometry preclude such measurements.

Recently, a model-based reconstruction method has been developed to estimate the three-dimensional spray distribution using a limited number of views [20]. At

each axial location of interest, the transverse distributions are fitted with Gaussian curves, elliptical curves, or the sum of two of these. The Gaussian curve represents the projection of a Gaussian density distribution, while an elliptical curve represents the projection of a constant-density core region. The model parameters are compared for different viewing angles, allowing even highly asymmetric density distributions to be determined. While this method relies on *a priori* specifying a form of the projection, and hence lacks the generality of true tomography, it has proved to be tractable, flexible, and effective for diesel sprays, especially at positions farther away from the nozzle.

To illustrate the influence of ambient density on the detailed spray distribution, two sprays at the same injection conditions (1100 bar injection pressure, 700 µs commanded injection duration) are tested at two different ambient density values (5.6 and 22.5 kg/m^3). For each measurement, the spray is measured at four different orientations. It should be noted that these measurements show only the liquid density, not the combined liquid and gas density.

Figure 8 shows the spray distribution near the nozzle exit (x = 0.1 mm) at 22.5 kg/m^3 ambient density. For this position, the underlying spray distribution was assumed to be an elliptically-shaped, constant density region. The derived distribution is nearly circular, with a mean diameter of 108 µm, which matches quite well the nominal nozzle diameter of 110 µm. The derived density is 790 kg/m^3, compared to a bulk liquid density of 884 kg/m^3. This distribution closely matches the expected behavior at the nozzle exit, i.e. nearly circular distribution whose density is close to the bulk liquid density. Similar behavior is expected for the 5.6 kg/m^3 case.

While the exit density profile is nearly symmetric, the spray exhibits significant asymmetries farther downstream. The spray distributions at x^* = 5.8 for 5.6 kg/m^3 and 22.5 kg/m^3 ambient density are shown in Figs. 9 and 10, respectively. Both sprays show severe asymmetry. The assumed form of the distribution for the reconstruction is the sum of two elliptically-shaped Gaussian distributions. The resulting reconstructions exhibit a broad, low density sheath punctuated by a narrow, high density core. The peak density of both distributions is also similar, at around 400 kg/m^3. This density value suggests that the spray core is not purely liquid. On the other hand, if the spray core consists of spray droplets, they must exist in exceedingly close proximity to each other. The distributions also show marked differences from each other. The sheath distribution is more asymmetric, but the core distribution is more circular, for the 5.6 kg/m^3 ambient density vs. 22.5 kg/m^3 ambient density. Note that the major axes of the spray distributions are aligned in the same orientation for x = 0.1 and x* = 5.8 (Figures 8-10).

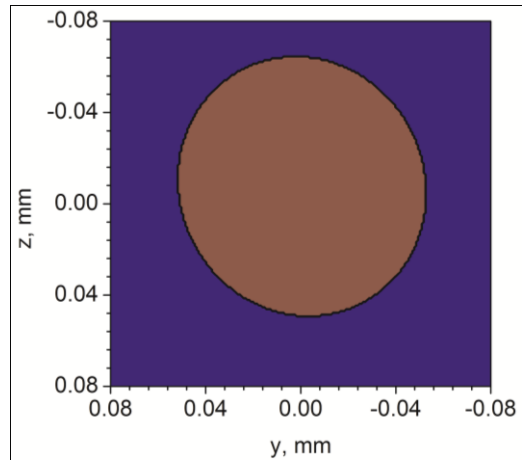

Figure 8. Spray distribution at x = 0.1 mm for 22.5 kg/m^3 ambient density.

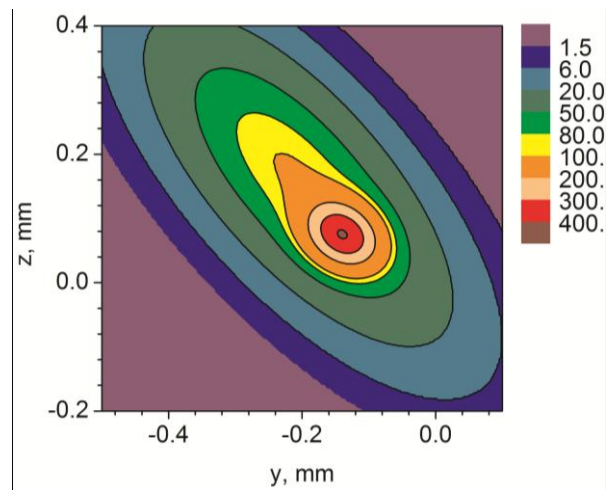

Figure 9. Spray density distribution at x^* = 5.8 for 5.6 kg/m^3 ambient density.

The behavior of the sprays changes significantly with downstream distance. At x^* = 8.7 (Figs. 11 and 12), the behavior is similar to that seen at x* = 5.8, with a broadening of the sheath region, particularly for the 5.6 kg/m^3 case. At x* = 11.6, the sheath for 5.6 kg/m^3 ambient density has become quite broad and dilute. The amount of mass in the sheath region remains largely constant as x^* increases for 5.6 kg/m^3 ambient density, whereas the sheath region mass increases significantly as x^* increases at 22.5 kg/m^3 ambient density. The peak density of both distributions at x* = 11.6 is less than 100 kg/m^3, representing a liquid volume fraction of less than 12%. It seems likely at this position that the spray has broken up significantly, though if the spray consists of discrete droplets, they must reside in close proximity in the highest density regions.

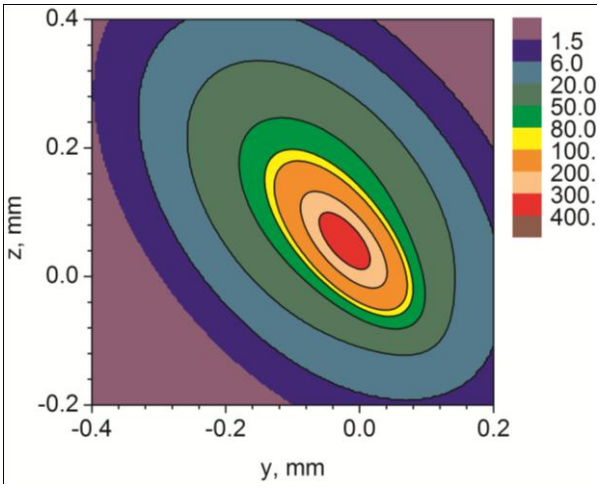

Figure 10. Spray density distribution at x^* = 5.8 for 22.5 kg/m^3 ambient density.

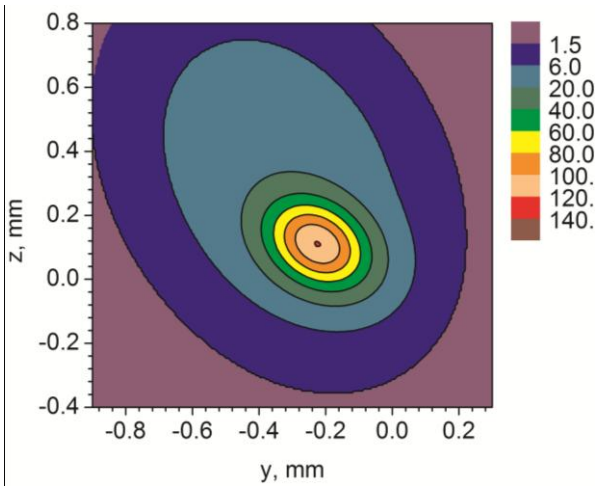

Figure 11. Spray density distribution at x^* = 8.7 for 5.6 kg/m^3 ambient density.

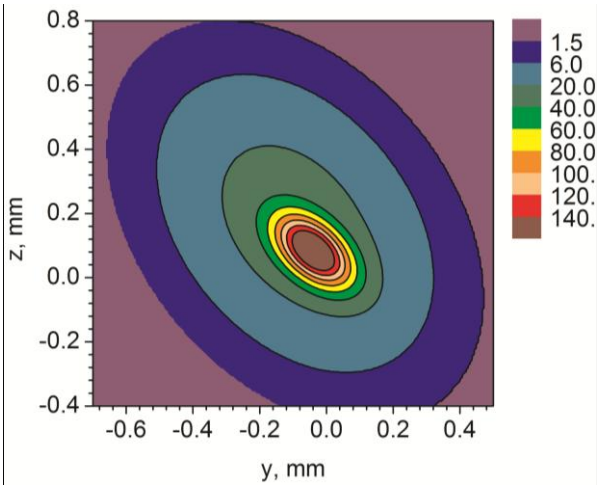

Figure 12. Spray density distribution at x^* = 8.7 for 22.5 kg/m^3 ambient density.

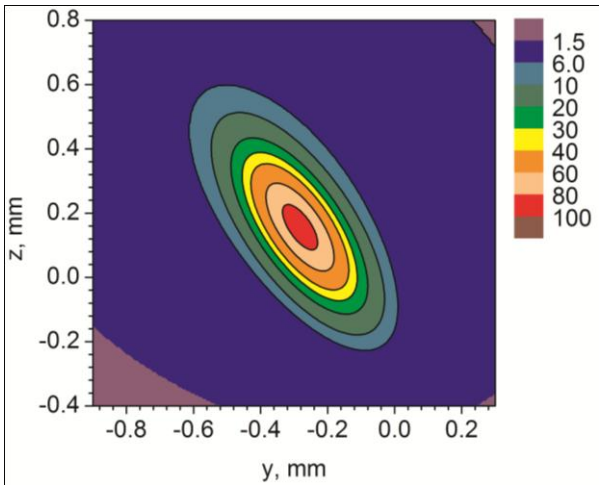

Figure 13. Spray density distribution at x^* = 11.6 for 5.6 kg/m^3 ambient density.

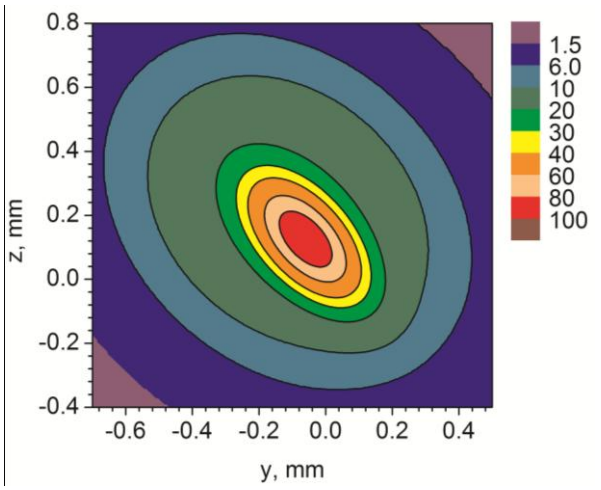

Figure 14. Spray density distribution at x^* = 11.6 for 22.5 kg/m^3 ambient density.

Multi-view measurements have been obtained farther downstream for the 5.6 kg/m^3 ambient density, but not the 22.5 kg/m^3 case. The spray distributions at x^* = 14.5 and 21.7 are shown in Figs. 15 and 16, respectively. As the spray progresses further downstream, the sheath region expands greatly, creating a large, dilute region of the spray. The core region also expands, albeit more slowly. The core density also decreases significantly; at x^* = 21.7, the peak liquid density is 17 kg/m^3, representing a liquid volume fraction of only 2%. The orientation of the major axis of the sheath remains constant throughout the axial development of the jet. At x^* = 21.7, the core region major axis is rotated somewhat compared to more upstream positions. The cause for this change in orientation is unclear.

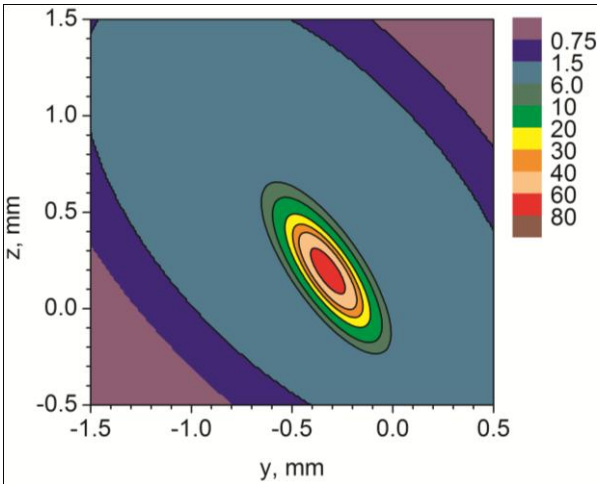

Figure 15. Spray density distribution at $x^* = 14.5$ for 5.6 kg/m^3 ambient density.

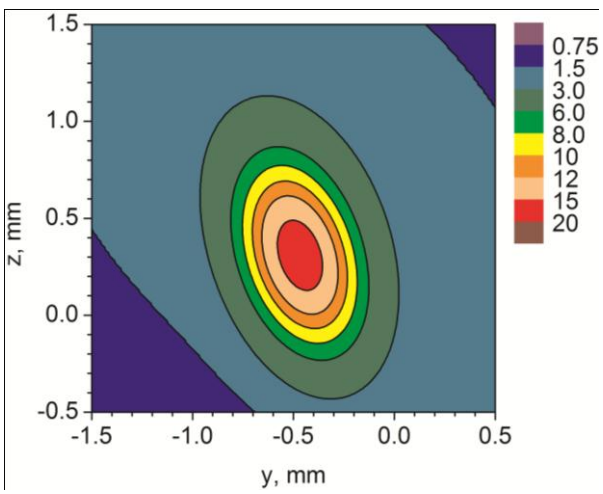

Figure 16. Spray density distribution at $x^* = 21.7$ for 5.6 kg/m^3 ambient density.

Spray Velocity Trends

An important aspect of the development of turbulent jets is the decrease in axial velocity with distance from the nozzle. In single-phase jets [18], the axial velocity scales with $1/x$ in the fully-developed region.

Radiography measurements can be used to probe the trends in axial velocity at steady-state. This analysis is based on the transverse integrated mass (TIM), an integration of the projected density conducted transverse to the spray axis. The TIM gives the amount of mass present per unit length in the axial direction. As shown elsewhere [14], by continuity, the TIM at a particular axial location is inversely proportional to the mass-averaged axial velocity at that axial location. While this analysis only gives ratios between velocities (rather than absolute values), is limited to steady-state operation, and is mass-averaged across a cross-section, it remains useful in analyzing the spray development.

The TIM vs. x at steady-state is shown for 700 bar and 1100 bar injection pressure for 5.6 and 22.5 kg/m^3 ambient density in Fig. 17. As expected, the TIM increases monotonically as the jet progresses downstream, indicating that the jet is decelerating. This development is far more rapid at higher ambient density, as shown in previous measurements [14].

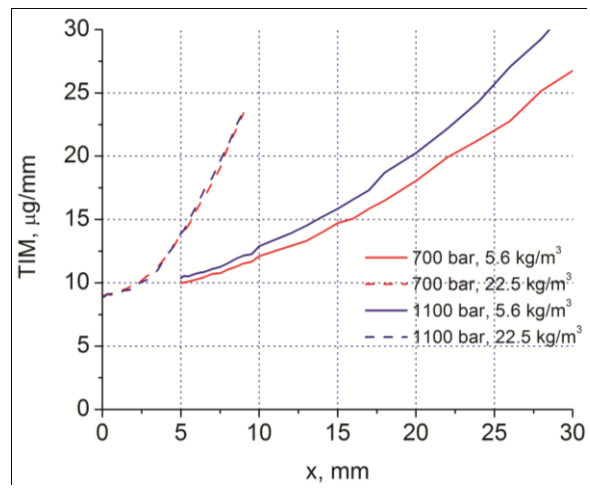

Figure 17. TIM vs. x at steady-state for four different injection conditions.

Figure 18 shows the trends in spray velocity derived from the TIM plotted against the rescaled axial coordinate. The behavior of the current sprays is quite similar to what seen in previous work [14]. The axial rescaling accounts for much of the difference in spray velocity development as ambient density changes. However, even with the rescaling, the jet still develops more slowly for the lower ambient density case. Another interesting trend is that while the spray velocity trends show little dependence on injection pressure at high ambient density, they do depend on injection pressure at low ambient density.

Discussion

One of the more puzzling aspects of the current work is the behavior of the low ambient density sprays at more downstream positions. In contrast to the high ambient density measurements, the low ambient density sprays seem not to be as strongly impacted by the ambient gas, even when accounting for the density ratio effects. The density distributions maintain the asymmetries seen in the near-nozzle region farther downstream, and the velocity decays more slowly than at higher ambient density.

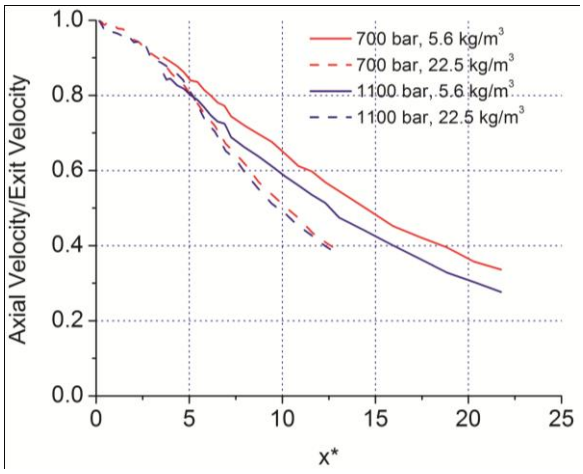

Figure 18. Ratio between local mass-averaged axial velocity and exit velocity as a function of x^*.

The axial rescaling based on the density ratio is motivated by a momentum argument. Normally, the axial coordinate of a jet is scaled by the nozzle diameter. Rescaling this diameter by the square root of the density ratio gives the nozzle diameter that yields an equivalent jet momentum to the variable density jet assuming that the injected fluid is the same density as the ambient and injected at the same velocity as the variable density jet. A closer examination of the spray dynamics may shed light on the deficiencies of this rescaling. Consider the behavior of an isolated droplet penetrating into a stagnant ambient gas. The drag force on a droplet of diameter d is given by:

$$F_D = \frac{1}{6}\rho V^2 \pi d^2 C_D \tag{3}$$

If one assumes that the drag coefficient remains constant, the expression for deceleration caused by drag is given by:

$$a = \frac{dV}{dt} = \frac{3C_D \rho_g V^2}{4d\rho_\ell} \tag{4}$$

Integrating for the velocity and position (assuming an initial position $x = 0$ and an initial velocity V_0) gives the expressions:

$$V = B\left(t + \frac{B}{V_0}\right)^{-1} \tag{5}$$

$$x = B \ln\left(\frac{tV_0}{B} + 1\right) \tag{6}$$

$$B = \frac{4d\rho_\ell}{3C_D \rho_g}$$

Note that the decay in velocity as well as the position where the velocity decays to a given fraction of its initial value depends on B, which is directly proportional to the density ratio, not the square root of the density ratio. If this process of the droplet velocity decay significant changes the spray dynamics, it will tend to make sprays more sensitive to ambient density changes than the aforementioned axial rescaling would indicate. This would make spray interactions with the ambient gas less vigorous than expected at low ambient density. Admittedly, a diesel spray consists of a large number of droplets interacting both with each other and inducing significant ambient gas velocities, not isolated droplets in a stagnant environment. Nevertheless, the linear dependence between the velocity decay due to drag and the density ratio may explain the inability of axial rescaling based on the density ratio to account for all of the dependence of spray behavior on ambient density.

Another peculiar behavior seen in the current data is the dependence of velocity decay on injection pressure. Previous radiography measurements have generally shown little or no impact of injection pressure on steady-state spray structure. Such behavior is not surprising; injection pressure influences the injection velocity and hence Reynolds number, and in a fully turbulent flowfield, Reynolds number effects are expected to be relatively minor.

There are three possible explanations for this behavior. First, the changes in ambient pressure may have altered the internal nozzle flowfield, particularly if cavitation is present. Second, given that the injection velocity is at or above the speed of sound of the ambient gas, compressible flow effects might cause different behavior at different ambient density. Finally, perhaps the flowfield is not fully turbulent at low ambient density due to the small orifice size and low ambient density, allowing Reynolds number effects to play a greater role than expected in a fully-turbulent flowfield. The authors suspect that these differences are a Reynolds number effect, but more measurements are needed to confirm this hypothesis.

Another important insight from this work concerns the rate at which the jets approach self-similarity. The current measurements indicate that even at $x^* = 22$ (270 d_0 at 5.6 kg/m^3, 135 d_0 at 22.5 kg/m^3), the jet density profiles are still evolving significantly, both in qualitative shape and quantitative density values. This indicates that more axial distance is required before the jet can be considered fully-developed in terms of its density profile.

The shape of the three-dimensional spray distributions is also worthy of note. Previous reconstructions[20] have shown that the spray consists of a low density sheath and a relatively dense core, as has been seen in the sprays in this work. A truly axisymmetric spray would be instructive to determine whether this structure is a fundamental feature of diesel sprays or is an artifact of the asymmetric spray.

Conclusions

X-ray radiography has been used to examine sprays from an axial single-hole nozzle over a range of injection pressure and ambient density. An expanded field of view over previous x-ray radiography measurements has allowed both low and high ambient density measurements to be compared across an equivalent range of their axial development. The mass distributions show significant asymmetries, presumably due to imperfections in the nozzle geometry. Reconstructions of the three-dimensional spray structure show that the spray consists of a diffuse sheath surrounding a relatively dense core region. Rescaling the axial coordinate to account for the density ratio effects accounts for much of the influence of ambient density on spray structure. However, the lower ambient density case spreads more slowly and has a slower velocity decay even after the axial rescaling.

Acknowledgements

The submitted manuscript has been created by UChicago Argonne, LLC, Operator of Argonne National Laboratory ("Argonne"). Argonne, a U.S. Department of Energy Office of Science laboratory, is operated under Contract No. DE-AC02-06CH11357. . The U.S. Government retains for itself, and others acting on its behalf, a paid-up nonexclusive, irrevocable worldwide license in said article to reproduce, prepare derivative works, distribute copies to the public, and perform publicly and display publicly, by or on behalf of the Government.

This research was performed at the 7-BM beamline of the Advanced Photon Source, Argonne National Laboratory. The authors thank Gurpreet Singh and the U. S. Department of Energy Vehicle Technologies Program for their support of this work.

References

[1] Chang, C. and Farrell, P., "A Study of the Effects of Fuel Viscosity and Nozzle Geometry on High Injection Pressure Diesel Spray Characteristics," SAE Paper 970353, 1997.

[2] Holguin, A. and Foster, D., "Investigation of MicroFlow Machining Effects on Diesel Injector Spray Characteristics," SAE Paper 2004-01-0026, 2004.

[3] Naber, J. and Siebers, D., "Effects of Gas Density and Vaporization on Penetration and Dispersion of Diesel Sprays," SAE Paper 960034, 1996.

[4] Andriani, R., Coghe, A., and Cossali, G., "Near-field Entrainment in Unsteady Gas Jets and Diesel Sprays: A Comparative Study," 26th Symposium (International) on Combustion, The Combustion Institutue, 1996, pp. 2549-2556.

[5] Sánchez, M., Castro, F., Tinaut, G., and Melgar, A., "Considerations on the Gas-Phase Velocity Field in a Nonevaporating Diesel Spray," *Atomization and Sprays*, v. 10, 2000, pp. 529-543.

[6] Chaves, H., Kirmse, C., and Obermeier, F., "Velocity Measurements of Dense Diesel Fuel Sprays in Dense Air," *Atomization and Sprays*, v. 14, 2004, pp. 589-609.

[7] Leick, P., Bittlinger, G., and Tropea, C., "Velocity Measurements in the Near Nozzle Region of Common-Rail Diesel Sprays at Elevated Back-Pressures," 19th Annual ILASS-Europe Conference, Nottingham, UK, September 2004.

[8] Schmidt, J., Schaefer, Z., Meyer, T., Roy, S., Danczyk, S., and Gord, J., "Ultrafast time-gated ballistic-photon imaging and shadowgraphy in optically dense rocket sprays," *Applied Optics*, v. 48, n. 4, February 2009, pp. B137-B144.

[9] Kastengren, A., Powell, C. F., Im, K.-S., Wang, Y.-J., and Wang, J., "Measurement of Biodiesel Blend and Conventional Diesel Spray Structure Using X-Ray Radiography," *ASME Journal of Engineering for Gas Turbines and Power*, v. 131, November 2009, Paper 062802.

[10] Cai, W., Powell, C. F., Yue, Y., Narayanan, S., Wang, J., Tate, M., Renzi, M., Ercan, A., Fontes, E., and Gruner, S., "Quantitative Analysis of highly transient fuel sprays by time-resolved x-radiography," *Applied Physics Letters*, v. 83, n. 8, 2003, pp. 1671-1673.

[11] Hiroyasu, H., and Arai, M., "Structures of Fuel Sprays in Diesel Engines," SAE Paper 900475, 1990.

[12] Araneo, L, Coghe, A., Brumello, G., and Cossali, G., "Experimental investigation of gas density effects on diesel spray penetration and entrainment," SAE Paper 1999-01-0525, 1999.

[13] Wu, K.-J., Su, C.-C., Steinberger, R., Santavicca, D., and Baracco, F., "Measurements of the spray angle of atomizing jets," *Journal of Fluids Engineering*, v. 105, 1983, pp. 406-413.

[14] Kastengren, A., Powell, C. F., Wang, Y.-J, Im, K.-S., and Wang, J., "X-Ray Radiography Measurements of Diesel Spray Structure at Engine-Like Ambient Density," *Atomization and Sprays*, v. 19, November 2009, pp. 1031-1044.

[15] Pitts, W., "Effect of global density ratio on the centerline mixing behavior of axisymmetric turbulent jets," *Experiments in Fluids*, v. 11, n. 2-3, 1991, pp. 125-134.

[16] Kastengren, A., Powell, C. F., Arms, D., Dufresne, E. M., and Wang, J., "Spray Diagnostics at the Advanced Photon Source 7-BM Beamline," 23rd Annual ILASS-Americas Conference, Cincinnati, OH, May 2009.

[17] Eng, P., Newville, M., Rivers, M., and Sutton, S., "Dynamically Figured Kirkpatrick Baez X-Ray Micro-Focusing Optics," SPIE Conference on X-ray Microfocusing: Applications and Techniques," San Diego, CA, July 1998

[18] Pope, S. *Turbulent Flows*, Cambridge University Press, Cambridge, 2000.

[19] Kak, A. and Slaney, M., *Principles of Computerized Tomographic Imaging*, IEEE Press, New York, 1988, p. 186.

[20] Kastengren, A., Powell, C. F., Liu, Z., and Wang, J., "Time-Resolved, Three Dimensional Mass Distributions of Diesel Sprays Measured with X-Ray Radiography," SAE Paper 2009-01-0840, 2009.